AGU ADVANCING EARTH AND SPACE SCIENCES

AGU Advances

RESEARCH ARTICLE
10.1029/2024AV001187

Peer Review The peer review history for this article is available as a PDF in the Supporting Information.

Key Points:

- The total carbon loss caused by the 2015–2016 El Nino had not recovered by the end of 2018
- The slow recovery is attributed to the unexpected carbon loss caused by severe atmospheric aridity and water storage deficit during drought
- The attenuation of carbon uptake is three times higher than expected from the pre-drought carbon-climate sensitivity

Supporting Information:

Supporting Information may be found in the online version of this article.

Correspondence to:

J. Liu,
junjie.liu@jpl.nasa.gov

Citation:

Liu, J., Bowman, K., Palmer, P. I., Joiner, J., Levine, P., Bloom, A. A., et al. (2024). Enhanced carbon flux response to atmospheric aridity and water storage deficit during the 2015–2016 El Niño compromised carbon balance recovery in tropical South America. *AGU Advances*, *5*, e2024AV001187. https://doi.org/10.1029/2024AV001187

Received 15 JUL 2022
Accepted 4 JUL 2024

Author Contributions:

Conceptualization: Junjie Liu
Data curation: Junjie Liu, Paul I. Palmer, Joanna Joiner, Paul Levine, A. Anthony Bloom, Liang Feng
Formal analysis: Junjie Liu
Funding acquisition: Junjie Liu, Kevin Bowman, Paul I. Palmer
Investigation: Junjie Liu, Kevin Bowman, Paul I. Palmer, Joanna Joiner, Paul Levine, A. Anthony Bloom, Sassan Saatchi, Michael Keller, Marcos Longo, David Schimel, Paul O. Wennberg

Enhanced Carbon Flux Response to Atmospheric Aridity and Water Storage Deficit During the 2015–2016 El Niño Compromised Carbon Balance Recovery in Tropical South America

Junjie Liu[1,2], Kevin Bowman[1,3], Paul I. Palmer[1,4], Joanna Joiner[5], Paul Levine[1], A. Anthony Bloom[1], Liang Feng[4,6], Sassan Saatchi[1], Michael Keller[1,7], Marcos Longo[1,8], David Schimel[1], and Paul O. Wennberg[2]

[1]NASA Jet Propulsion Laboratory, California Institute of Technology, Pasadena, CA, USA, [2]California Institute of Technology, Pasadena, CA, USA, [3]Joint Institute for Regional Earth System Science and Engineering, University of California Los Angeles, Los Angeles, CA, USA, [4]National Centre for Earth Observation, University of Edinburgh, Edinburgh, UK, [5]Goddard Space Flight Center, Greenbelt, MD, USA, [6]School of GeoSciences, University of Edinburgh, Edinburgh, UK, [7]USDA Forest Service, International Institute of Tropical Forestry, San Juan, PR, USA, [8]Now at Climate and Ecosystem Sciences Division, Lawrence Berkeley National Laboratory, Berkeley, CA, USA

Abstract During the 2015–2016 El Niño, the Amazon basin released almost one gigaton of carbon (GtC) into the atmosphere due to extreme temperatures and drought. The link between the drought impact and recovery of the total carbon pools and its biogeochemical drivers is still unknown. With satellite-constrained net carbon exchange and its component fluxes including gross primary production and fire emissions, we show that the total carbon loss caused by the 2015–2016 El Niño had not recovered by the end of 2018. Forest ecosystems over the Northeastern (NE) Amazon suffered a cumulative total carbon loss of ∼0.6 GtC through December 2018, driven primarily by a suppression of photosynthesis whereas southeastern savannah carbon loss was driven in part by fire. We attribute the slow recovery to the unexpected large carbon loss caused by the severe atmospheric aridity coupled with a water storage deficit during drought. We show the attenuation of carbon uptake is three times higher than expected from the pre-drought sensitivity to atmospheric aridity and ground water supply. Our study fills an important knowledge gap in our understanding of the unexpectedly enhanced response of carbon fluxes to atmospheric aridity and water storage deficit and its impact on regional post-drought recovery as a function of the vegetation types and climate perturbations. Our results suggest that the disproportionate impact of water supply and demand could compromise resiliency of the Amazonian carbon balance to future increases in extreme events.

Plain Language Summary The carbon storage in tropical South America (SA, 15°S−10°N) is equivalent to approximately one third of the carbon currently residing in the atmosphere. The future durability of this carbon reservoir is very uncertain, contributing significantly to the uncertainties of the global carbon cycle predictions. The soil and the overlying atmosphere of tropical SA is expected to become drier in the future so it is critical we understand how the carbon cycle will respond to this combined atmospheric and soil drought. Using several carbon flux quantities that are constrained by satellite observations, we quantified the recovery of total carbon loss after the 2015–2016 drought at regional scale. Our work sheds light on how the combined effect of atmosphere dryness and soil drought exacerbates the impact of either atmosphere dryness or soil drought alone and delays the recovery of total carbon storage after the drought. Consequently, our study suggests that tropical SA may eventually become a source of carbon to the atmosphere due to increasing drought events and decreasing soil water storage, instead of its current net carbon-neutral state.

1. Introduction

With the carbon storage equivalent to approximately one third of the carbon currently residing in the atmosphere (S. S. Saatchi et al., 2011), tropical South America (SA, 15°S−10°N) is a primary contributor to the uncertainties of the global carbon cycle predictions (Bonan et al., 2019) (IPCC AR5, Chapter 6). The large carbon stock and poor understanding of the sensitivity of biogeochemical processes to climate stressors highlight the need to better understand the carbon dynamics over the region. In response to the 2015–2016 El Niño, this region experienced

Methodology: Junjie Liu, Kevin Bowman, Paul I. Palmer, Joanna Joiner, Paul Levine, A. Anthony Bloom
Resources: Junjie Liu
Software: Junjie Liu
Validation: Junjie Liu, Kevin Bowman
Visualization: Junjie Liu, Kevin Bowman, Paul I. Palmer, Paul O. Wennberg
Writing – original draft: Junjie Liu, Kevin Bowman, Paul I. Palmer
Writing – review & editing: Junjie Liu, Kevin Bowman, Paul I. Palmer, Joanna Joiner, Paul Levine, A. Anthony Bloom, Liang Feng, Sassan Saatchi, Michael Keller, Marcos Longo, David Schimel, Paul O. Wennberg

high temperatures coupled with one of the most severe and enduring droughts on record (Jimenez et al., 2018). Compared to the previous 2005 and 2010 Amazonian drought, the drought-stricken area was most widespread in 2015–2016. The associated reduction of above ground biomass due to this drought had not recovered by the end of 2017 (Wigneron et al., 2020); at which time it is also unclear whether the total carbon loss (including both the above and below ground biomass and soil carbon) had recovered. In spite of a rich literature that has investigated the impact of drought and its recovery on the above ground biomass with plot and remote sensing data over the Amazon (Lewis et al., 2011; Phillips et al., 2009; S. Saatchi et al., 2013), studies that quantify the recovery of total carbon loss after drought at regional scale are largely absent from the literature. As the 2015–2016 drought was such a large perturbation to the ecosystem, it is critically important to understand the link between the drought impact and recovery of the total carbon pools and its biogeochemical drivers.

While precipitation is a key measure of drought, the balance of water supply indicated by total water storage (TWS) and atmospheric water demand represented by vapor pressure deficit (VPD; difference between saturation and actual water vapor pressure) can have a more direct impact on plant functioning (Sulman et al., 2016). In particular, increasing VPD tends to suppress photosynthesis and stimulate transpiration over wet tropics (Grossiord et al., 2020). While ground water can act as a buffer on atmospheric demand, under prolonged or severe drought, TWS could be greatly reduced. High VPD coupled with large reductions in TWS can accelerate tree mortality through either hydraulic failure or carbon starvation (Bonal et al., 2016; Breshears et al., 2013). Over tropical SA, VPD has increased in recent decades (Barkhordarian et al., 2019) and is projected to continue increasing (Jensen et al., 2020), while TWS is projected to decrease (Y. Pokhrel et al., 2021). Consequently, it is crucial to enhance our understanding of how the sensitivity of carbon fluxes to atmospheric aridity can change, particularly in conjunction with TWS anomalies, and how these factors collectively contribute to carbon flux anomalies during drought and subsequent recovery. Assessing these aspects is essential for mitigating uncertainties associated with carbon-climate feedbacks (Barkhordarian et al., 2021; Cook et al., 2019; Ukkola et al., 2020).

The tropical SA exhibits a remarkable diversity of plant types, shaped by varying mean climates and a complex history of human impact. Covering about two-thirds of the area, the Amazon rainforests boast a significantly wetter climate compared to the Cerrado region, which occupies most of the remaining one-third and is characterized by savannas and dry forests. Recent trends in deforestation rates highlight contrasting patterns between these regions, with the Amazon experiencing a decrease in deforestation while the Cerrado is seeing an alarming increase, primarily due to demographic pressures and expanding agriculture. Furthermore, the role of fires in these ecosystems differs substantially; while fire is not a natural disturbance mechanism in the Amazon, the Cerrado has evolved with fire-adapted vegetation and is naturally prone to fires. Even within the Amazon, there are pronounced variations in drought severity in 2015–2016. For instance, the northeast region experienced the most severe drought in 2015–2016 (Jiménez-Muñoz et al., 2016) and is predicted to become significantly drier compared to the rest of the Amazon (Baker et al., 2021). These distinctions suggest that the response of these regions to droughts and subsequent recovery would be regionally distinct (Stuart-Haëntjens et al., 2018). To better understand these nuances and dependencies, we divide tropical South America into three sub-regions: (a) the northeast (NE-Amazon) and (b) the west and southwest (WSW-Amazon) moist tropical rainforest, and (c) the southeast dry tropical forest and savanna (SE-Savanna) (Figure S1 in Supporting Information S1). The NE-Amazon includes those grid points over the northeast part of the Amazon Forest that have annual mean precipitation less than 5 mm/day and the VPD variability more than 0.4 hPa, with a few exceptional points over each region to ensure continuity (Figures S1 and S2 and Table S1 in Supporting Information S1). The SE-Savanna includes the Cerrado region. Among these three regions, the precipitation variability in the NE-Amazon has the highest correlation ($r = 0.6$) with the Oceanic Nino index, implying a stronger teleconnection with El Nino Southern Oscillation (ENSO) cycle, while the SE-Savana has the lowest correlation ($r = 0.2$).

Previous studies assessing the impact of drought and its recovery in the Amazon have primarily relied on precipitation throughfall experiments (Brando et al., 2019; da Costa et al., 2010; Meir et al., 2009), along with limited plot data and aboveground biomass data inferred from remote sensing (Lewis et al., 2011; Phillips et al., 2009; S. Saatchi et al., 2013; Wigneron et al., 2020). Satellite-based net biosphere exchange (NBE, the net carbon flux from all land–atmosphere exchange processes except fossil fuel emissions) and its component fluxes provide a complementary viewpoint allowing us to quantify total carbon pool changes at the subregional scale over tropical SA. Using 9-years (2010–2018) of monthly satellite-constrained NBE estimates and their component fluxes (i.e., Gross Primary Production (GPP), ecosystem respiration and wildfire emissions), we aim to address the following

scientific questions: (a) Has the total carbon loss caused by the 2015–2016 El Niño recovered by December 2018? (b) Has the response been enhanced by the compound effect of atmospheric aridity and water storage deficit? (c) How does the carbon cycle response to synergistic anomalies in water supply and atmospheric water demand during drought and recovery vary among the three sub-regions and what biophysical processes cause these differences among sub-regions? By investigating the heterogeneity of carbon cycle responses to drought and recovery and examining the dependency of carbon-climate sensitivities on climate perturbations and vegetation types in these sub-regions, we aim to gain deeper insights into the complex dynamics of these ecosystems. Our understanding of the 2015–2016 drought impact caused by El Niño may also offer valuable perspectives into the effect of the current (2023–2024) Amazonian drought on the carbon cycle.

2. Materials and Methods

2.1. Observation-Constrained NBE, Fire, GPP and Proxies, and Total Ecosystem Respiration

Carbon fluxes used in this study including NBE, GPP, and fire emissions have previously been described in detail (Bowman et al., 2017; Joiner et al., 2018; Liu et al., 2020; Palmer, Feng, & Baker, 2019). We used two NBE products inferred from atmospheric top-down flux inversions, CMS-Flux-NBE 2020 (Liu et al., 2020) and GEOS-Chem-EnKF (Palmer, Feng, Baker, Chevallier, et al., 2019), constrained by satellite column CO_2 (X_{CO2}) retrievals from GOSAT (version ACOS v7.3) and OCO-2 (version b9) (O'Dell et al., 2018); both products cover January 2010–December 2018. CMS-Flux estimates NBE and its uncertainty with a 4D-Variational (4D-Var) and a Monte Carlo method (Liu et al., 2014, 2020), while GEOS-Chem-EnKF calculates NBE and its uncertainty with an ensemble Kalman filter (Feng et al., 2009; Palmer, Feng, Baker, Chevallier, et al., 2019). Both top-down inversion methods utilize atmospheric transport model GEOS-Chem to link surface carbon fluxes with atmospheric CO_2 concentration and adjust the assumed prior fluxes to best match the observed CO_2 concentration, given the prescribed uncertainties in both observations and prior fluxes. Both CMS-Flux and GEOS-Chem-EnKF have been extensively evaluated against independent aircraft observations (Liu et al., 2020). We calculated the mean NBE of these two products, with its uncertainties equal to the squared sum of the estimated uncertainties from both products.

We estimated CO_2 fluxes from fire and their uncertainty with the CMS-Flux inversion system (Bowman et al., 2017; Liu et al., 2017) by assimilating carbon monoxide (CO) retrievals from MOPITT (Deeter, 2018). CO is an excellent tracer for fire carbon emissions because of its relatively shorter lifetime (about a month) than CO_2. The estimated fire CO emissions were converted to CO_2 emissions using the CO_2:CO emission ratios derived from field and lab experiments (Bowman et al., 2017; Liu et al., 2017). Both fire CO_2 fluxes and posterior NBE are monthly temporal resolution at 4° (latitude) × 5° (longitude) spatial resolution.

We used the daily FluxSAT GPP product (Joiner & Yoshida, 2020; Joiner et al., 2018), which was generated by a machine learning method using GPP data from flux towers (Pastorello et al., 2020), MODIS reflectance, solar induced chlorophyll fluorescence (SIF) from TROPOMI, and ancillary meteorological data that includes 2-m temperature, humidity and surface pressure (from MERRA2 reanalysis). The uncertainty in GPP assigned by FluxSAT reflects the differences between the predicted GPP from the machine learning algorithm and the GPP measurements obtained at the flux tower sites (Joiner & Yoshida, 2020). The product captures the daily, seasonal, and interannual variability of GPP measurements from flux towers. To further support the analysis based on FluxSAT GPP, we also analyzed OCO-2 SIF measurements (September 2014-onward), MODIS NIRv, and GPP from the one Amazon flux tower site that had a drought event lasting longer than 12 months. SIF is a by-product of photosynthesis, and has been shown to be linearly correlated with GPP on monthly time scale (Frankenberg et al., 2011; Sun et al., 2017) and with NBE over the Amazon (Parazoo et al., 2013). NIRv is the product of the normalized difference vegetation index (NDVI) and near infrared reflectance. NIRv explains a large fraction of the variance of GPP on monthly to annual time scales (Badgley et al., 2017; Ryu et al., 2019).

Following Liu et al. (2017) and Bowman et al. (2017), we calculated the total ecosystem respiration (TER) as:

$$\mathrm{TER} = \mathrm{NBE} + \mathrm{GPP} - \mathrm{fire} \quad (1)$$

TER, GPP, and fire are always positive, and positive NBE means releasing carbon from the biosphere to the atmosphere.

We regridded all the quantities to 4° (latitude) × 5° (longitude) spatial resolution before we calculated regional values over NE-Amazon, WSW-Amazon, and SE-Savanna using the same regional mask. We calculated the monthly climatology of carbon fluxes and the climate states using data between January 2010 and December 2018. The carbon flux anomalies represent the differences between monthly values and the monthly climatology, capturing the impacts of climate as well as other factors like forest degradation and human disturbances, which can also vary with climate perturbations. Understanding the interplay between these factors and the drought's impacts and recovery is crucial, but it requires data with much higher spatial resolution than what was used in this study.

We leveraged several satellite-constrained GPP, NBE, and fire emission data products that have been validated and calibrated in previous studies. Though validation of these data sets in representing regional carbon flux anomalies in tropical SA seemed to be lacking due to absence of ground truth at regional scales, whenever possible, we analyzed independent data sets throughout the paper to support the conclusions drawn from these data sets. For example, we showed that the conclusions drawn from GPP data are qualitatively consistent with those from SIF and GPP at a flux tower site. Satellite observations from multiple sources have become instrumental in understanding the impact of extreme events on carbon cycle from earth system standpoint. Yet, how to validate these satellite-derived fluxes at regional scales is still challenging, primarily due to the scale mismatch between site-level observations and regional impact of extreme events. Careful design of field experiments and ground site locations that are more representative of regional ecosystem function may pave the path for future validations of regional carbon fluxes.

2.2. The Timing of the 2015–2016 Drought Stages

The response of climate states and the resultant changes in terrestrial biosphere carbon fluxes over tropical SA generally lag sea surface temperature (SST) anomalies over the tropical Pacific Ocean during El Niño events (Kumar & Hoerling, 2003). We define the drought stages using a combination of the monthly FluxSAT GPP anomalies and the Nino 3.4 index (the mean SST anomaly over 5°N–5°S, 170°W–120°W).

Based only on Nino 3.4, the 2015–2016 El Niño started in April 2015 and ended in April 2016, when the Nino 3.4 exceeded 0.5°C for a period of six months or more. Putting that into the context of GPP anomalies, we define the start of the 2015–2016 drought as the first month when the regional GPP anomaly was negative for a period of at least 4 months between April 2015 and April 2016, and the ending of the 2015–2016 drought as the first month that the GPP anomaly was positive for a period of at least 4 months following the maximum Nino 3.4 index. Based on this refined definition, the starting and ending month of 2015–2016 drought depends on region (Table S3 in Supporting Information S1). Defining drought periods using precipitation anomalies produced results similar to using GPP (Figure S2 in Supporting Information S1), with discrepancies of less than 2 months. However, using GPP to define drought aligns better with the carbon cycle's response to climate extremes (Frank et al., 2015), as it can capture ecosystem responses to both water supply and atmospheric water demand anomalies. In contrast, defining drought using soil moisture or cumulative precipitation deficit anomalies may overlook GPP anomalies caused by atmospheric aridity.

The post-drought period extended from the end of the drought to December 2018. Finally, we defined the pre-drought from May 2012 until the start of the 2015–2016 drought. May 2012 was chosen as it was the first month after January 2010 that had an absolute Nino 3.4 index less than 0.5 (i.e., normal).

2.3. Changes of Carbon—Climate Sensitivities as a Function of Climate Anomalies and Their Contributions to Carbon Flux Anomalies During Drought and Post-Drought

To investigate whether the response of carbon flux to climate anomalies depend on the magnitude of climate anomalies, we calculated the sensitivities of carbon flux anomalies to climate state anomalies, including VPD, temperature, precipitation, and TWS, by fitting a linear model between monthly regional mean carbon flux anomalies (ΔC) and the monthly regional mean climate state anomalies (ΔM) at each drought stage (s)—pre-drought, drought, and post-drought:

$$\Delta \mathrm{C} = f_{r,s}(\Delta M) = a_{r,s}\,\Delta M + b_{r,s} \tag{2}$$

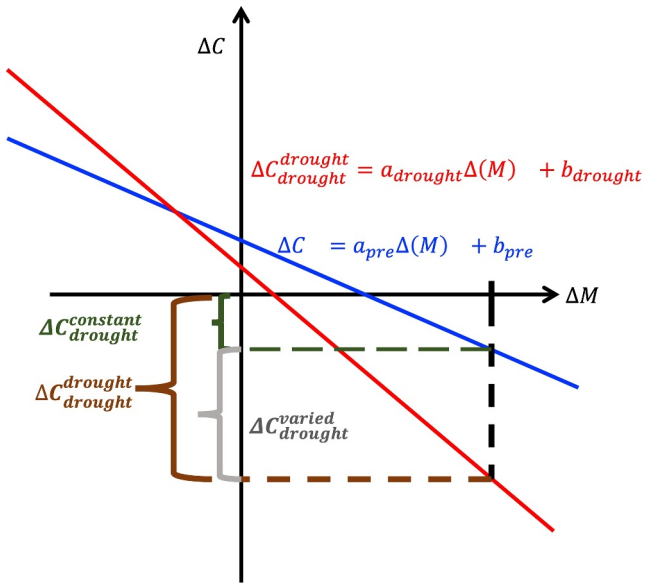

Figure 1. Schematic diagram to illustrate the impact of sensitivity changes on carbon flux anomalies during drought. $\Delta C^{\text{drought}}_{\text{drought}}$ is the carbon flux anomalies due to the drought climate anomalies and the carbon- sensitivities derived for the drought period $f_{\text{drought}}(\Delta M)$. $\Delta C^{\text{constant}}_{\text{post}}$ represents what carbon flux anomalies would be during drought under pre-drought carbon-climate sensitivity $f_{\text{pre}}(\Delta M)$. $\Delta C^{\text{varied}}_{\text{drought}}$ represents the carbon flux anomalies from changing sensitivities to climate anomalies (ΔM) and changes in reference carbon flux anomalies ($b_{\text{drought}} - b_{\text{pre}}$) between drought and pre-drought.

where ΔM represents monthly climate state anomalies (e.g., VPD) relative to a monthly climatology calculated over 2010–2018 for each region (Figure 1); $a_{r,s}$ is the fitted linear slope at region r for drought stage s, and $b_{r,s}$ is the corresponding intercept (Figure 1). We define the sensitivities of carbon flux anomalies to climate anomalies as a function of drought stage following Novick et al. (2016). We delineate carbon flux-climate sensitivities by soil moisture magnitude, effectively isolating the impacts of soil moisture variability from other climate states on the interannual variability of carbon fluxes. Values of $b_{r,s}$ represent the regional reference carbon flux anomalies that correspond to soil water anomalies during different drought stages. Values for the slope $a_{r,s}$ denote the sensitivity of carbon fluxes to climate anomalies ΔM. If the reference carbon flux anomalies are independent of drought stages and the sensitivity of carbon flux anomalies to climate anomalies remain constant with time, $a_{r,s}$ and $b_{r,s}$ would be the same across all drought stages. Otherwise, the response of carbon cycle to drought and recovery would depend on both climate anomalies and the changes of reference carbon flux anomalies due to water availability (Figure 1). The sample size for the linear fits is the same as the number of months during each drought stage over each region (Table S5 in Supporting Information S1).

We calculated the contributions of the changes in carbon—climate sensitivities to the drought response $\Delta C^{\text{varied}}_{\text{drought}}$ as:

$$\Delta C^{\text{varied}}_{\text{drought}} = \Delta C^{\text{drought}}_{\text{drought}} - \Delta C^{\text{constant}}_{\text{drought}}, \tag{3}$$

where $\Delta C^{\text{drought}}_{\text{drought}}$ is the carbon flux anomalies calculated from the linear carbon-climate sensitivity relationship derived for the drought period $f_{\text{drought}}(\Delta M)$, (Figure 1). It can be written as:

$$\Delta C^{\text{drought}}_{\text{drought}} = f_{\text{drought}}\left(\Delta(M)_{\text{drought}}\right) = a_{\text{drought}}\Delta(M)_{\text{drought}} + b_{\text{drought}} \tag{4}$$

where b_{drought} represents reference carbon flux anomalies during drought, and $a_{\text{drought}}\Delta(M)_{\text{drought}}$ represents carbon flux anomalies due to climate anomalies $\Delta(M)_{\text{drought}}$. We use $\Delta C^{\text{slope}}_{\text{drought}}$ to represent $a_{\text{drought}}\Delta(M)_{\text{drought}}$ and $\Delta C^{\text{reference}}_{\text{drought}}$ to represent b_{drought} in Table S4 of the Supporting Information S1.

$\Delta C^{\text{constant}}_{\text{drought}}$ represents carbon flux anomalies due to drought, assuming a stable carbon-climate sensitivity and an unchanged reference carbon flux anomalies state (i.e., under pre-drought carbon-climate sensitivity $f_{\text{pre}}(\Delta M)$), and $\Delta C^{\text{constant}}_{\text{drought}}$ can be written as:

$$\Delta C^{\text{constant}}_{\text{drought}} = f_{\text{pre}}\left(\Delta(M)_{\text{drought}}\right) = a_{\text{pre}}\Delta(M)_{\text{drought}} + b_{\text{pre}}. \tag{5}$$

Then $\Delta C^{\text{varied}}_{\text{drought}}$ can be further written as the sum of two terms:

$$\Delta C^{\text{varied}}_{\text{drought}} = \left(a_{\text{drought}} - a_{\text{pre}}\right)\Delta(M)_{\text{drought}} + \left(b_{\text{drought}} - b_{\text{pre}}\right), \tag{6}$$

where the first term, $\left(a_{\text{drought}} - a_{\text{pre}}\right)\Delta(M)_{\text{drought}}$, represents the carbon flux anomalies from changing sensitivities to climate anomalies (ΔM), and the second term $(b_{\text{drought}} - b_{\text{pre}})$ represents changes in reference carbon flux anomalies between drought and pre-drought. Here we simplify the notations by dropping region index r, since we use the same equations for all three regions.

Following the same strategy, we calculated the contributions of the changes in carbon—climate sensitivities to the drought recovery as:

$$\Delta C_{\text{post}}^{\text{varied}} = \Delta C_{\text{post}}^{\text{post}} - \Delta C_{\text{post}}^{\text{constant}} \quad (7)$$

where $\Delta C_{\text{post}}^{\text{post}}$ is the carbon flux anomalies due to the post-drought climate anomalies and the carbon- sensitivities derived for the post-drought period. It can be written as:

$$\Delta C_{\text{post}}^{\text{post}} = f_{\text{post}}\left(\Delta(M)_{\text{post}}\right) = a_{\text{post}}\Delta(M)_{\text{post}} + b_{\text{post}} \quad (8)$$

and $\Delta C_{\text{post}}^{\text{constant}}$ represents what carbon flux anomalies would be during post-drought under pre-drought carbon-climate sensitivity $f_{\text{pre}}(\Delta M)$. Similarly as Equation 6, $\Delta C_{\text{post}}^{\text{varied}}$ can be written:

$$\Delta C_{\text{post}}^{\text{varied}} = \left(a_{\text{post}} - a_{\text{pre}}\right)\Delta(M)_{\text{post}} + \left(b_{\text{post}} - b_{\text{pre}}\right) \quad (9)$$

A value of zero $\Delta C_{\text{drought}}^{\text{varied}}$ or $\Delta C_{\text{post}}^{\text{varied}}$ means that the sensitivity of carbon flux anomalies to climate anomalies does not change between the different drought stages and the reference carbon flux anomalies are not a function of drought stages (Figure 1). A nonzero value of $\Delta C_{\text{drought}}^{\text{varied}}$ or $\Delta C_{\text{post}}^{\text{varied}}$ indicates that carbon cycle response to drought and recovery is not only a function of climate anomalies $\Delta(M)$, but also a function of the changes in carbon-climate sensitivities.

2.4. BR-Sa3 Site Description and Data Set

The BR-Sa3 locates within the NE-Amazon region (3.02°S, 54.98°W), which is within LBA-ECO flux tower network. The data is available at (Saleska et al., 2013). In our analysis, we used the monthly VPD (VPD_F), GPP (GPP_NT_VUT_REF) and soil water content (SWC_F_MDS_1) stored in the full set data set that covers January 2000–December 2004.

2.5. Evaporation, Transpiration, Water Use Efficiency, and Land-Atmosphere Coupling

We further analyzed evaporation and transpiration data from GLEAM 3.5a (Martens et al., 2017) (https://www.gleam.eu/), and calculated the squared Pearson correlation coefficient (R^2) between evapotranspiration (ET) anomalies and VPD anomalies for each drought stage over the three regions. GLEAM calculated ET as a product between evaporative stress factor and potential evaporation. The evaporative stress factor was based on observations of the microwave Vegetation Optical Depth (VOD) and estimates of root-zone soil moisture. Potential evaporation was based on observations of surface net radiation, near surface air temperature, and wind. The microwave observations made the GLEAM data set advantageous over tropical regions more influenced by clouds (Miralles et al., 2020; Salazar-Martínez et al., 2022). Evaluation against ET products from eddy covariance towers showed that GLEAM ET has comparable or better performance than other available ET products over the tropics and SA (Melo et al., 2021; Salazar-Martínez et al., 2022). Furthermore, we only used ET interannual variabilities in this study which is more robust among different remote-sensing-based ET products than the absolute estimates (Pan et al., 2020).

We further calculated water use efficiency (WUE) as the ratio between GPP and transpiration, which describes the carbon fixed through photosynthesis by terrestrial ecosystems relative to the water lost through transpiration. The changes of WUE reflect the adaptive strategies to drought stress. Increasing WUE during drought can be an indicator of drought adaptation (Yang et al., 2016).

Evapotranspiration reflects water supply from the land surface, while VPD represents atmospheric dryness. Both quantities are influenced by temperature and precipitation, but changes in either ET or VPD can also affect the other, creating a land-atmosphere feedback loop. For instance, an increase in ET can lead to a decrease in VPD, whereas an increase of VPD may result in higher ET. Therefore, a higher value of R^2 between ET and VPD signifies more pronounced interactions between land processes and atmospheric dryness. This suggests that R^2 between ET and VPD can indicate the strength of the land-atmosphere coupling and feedbacks (Humphrey et al., 2021).

3. Results

3.1. The Response of Tropical SA Biosphere Carbon Cycle to the 2015–2016 Drought and Recovery

Our top-down NBE estimates indicate that the tropical SA land as a whole was close to carbon neutral (−0.01 ± 0.16 GtC/year) for the full study period 2010–2018 (Table S2 in Supporting Information S1), with annual fire emissions equal to 0.22 ± 0.03 GtC/year and the net ecosystem exchange (NEE = NBE − fire) equal to −0.21 ± 0.03 GtC/yea. This result is broadly consistent with the 0.29 ± 0.40 GtC/year net carbon flux estimate based on aircraft observations during the same time period (Gatti et al., 2021) and the bottom up inventories (Harris et al., 2021; Hubau et al., 2020; Phillips et al., 2017; Xu et al., 2021). Similar to the aircraft inversion results (Gatti et al., 2021), we find that the close-to-carbon-neutral tropical SA land is due to the compensation of carbon source over the northeast Amazon and the net carbon sink over the west Amazon (Table S2 in Supporting Information S1).

The 2015–2016 drought greatly reduced GPP and increased the net carbon release into the atmosphere across the three study regions (Figure 2). The loss of total carbon pools, measured as cumulative changes of NBE since the start of drought, had not been balanced by carbon uptake so that the cumulative emissions are positive over the NE-Amazon and SE-Savanna, but had recovered over the WSW-Amazon by the end of 2018 (Figure 2). This corresponds to different characteristics of drought over these three regions. The length of drought was comparable between the NE-Amazon and the WSW-Amazon, while the SE-Savanna experienced a longer drought period (Table S3 in Supporting Information S1). The NE-Amazon had the strongest increase in VPD and largest reductions in TWS during the drought, as precipitation was anomalously negative even before the start of 2015–2016 El Niño. Conversely, the WSW-Amazon had the weakest increase in VPD and smallest reductions in TWS, resulting from the above-average precipitation before the start of drought and a weaker precipitation anomaly during the drought (Figure S2 in Supporting Information S1). Consequently, among the three regions, the WSW-Amazon had the weakest cumulative reduction in GPP (−0.26 ± 0.11 GtC) and the smallest cumulative increase in NBE (0.16 ± 0.08 GtC) during the drought (Figure 2 and Table S4 in Supporting Information S1). It is also where the recovery of the total carbon pool was the fastest (Figure 2b). By December 2018, the accumulated NBE anomaly was close to zero (−0.07 ± 0.16 GtC accumulated NBE). In contrast, the NE-Amazon had a 0.62 ± 0.09 GtC cumulative increase in NBE and 0.51 ± 0.16 GtC cumulative reduction in GPP during the drought (Figure 2a). The cumulative NBE and GPP anomaly were −0.03 ± 0.12 and 0.23 ± 0.09 GtC, respectively, during the immediate post drought period (Table S4 in Supporting Information S1). The cumulative NBE anomaly was 0.59 ± 0.16 GtC during April 2015–December 2018, indicating that although the NBE and GPP fluxes returned to pre-drought levels by 2017 (Figure 2), the total carbon pools lost during the drought were not fully recovered by the end of 2018. The much faster recovery of ecosystem carbon fluxes than the biomass carbon pools were also observed in previous controlled burned experiments in Amazon (Brando et al., 2019). Note here we approximate the total carbon pool changes as cumulative NBE, ignoring the impact of changes of lateral carbon transport on the changes of carbon pools.

Over the SE-Savanna, the cumulative NBE anomaly was 0.25 ± 0.08 GtC during drought. Both GPP and total ecosystem respiration (TER) were reduced, with cumulative GPP reduced by 0.51 ± 0.11 GtC and cumulative TER reduced by 0.36 ± 0.20 GtC (Figure 2c). The fire anomaly was also the largest, with the cumulative 0.08 ± 0.01 GtC fire carbon emission during September 2015–June 2017, much larger than the 0.01 and −0.04 GtC cumulative fire carbon emission anomaly over the NE-Amazon and WSW-Amazon respectively. The cumulative NBE anomaly was −0.12 ± 0.03 GtC during the recovery period, and the cumulative NBE anomaly was 0.13 ± 0.16 GtC during September 2015–December 2018 (Figure 2c), implying that the total carbon stocks did not recover by the end of 2018. Since decreases of GPP and TER canceled each other to a large degree over the SE-Savanna, the cumulative NBE anomaly was dominated by the carbon loss from fire.

The cumulative NBE over the whole tropical SA was 0.65 ± 0.28 GtC by December 2018, indicating that the total carbon loss had not yet recovered to pre-drought conditions driven largely by GPP suppression in the NE-Amazon (Figure 2).

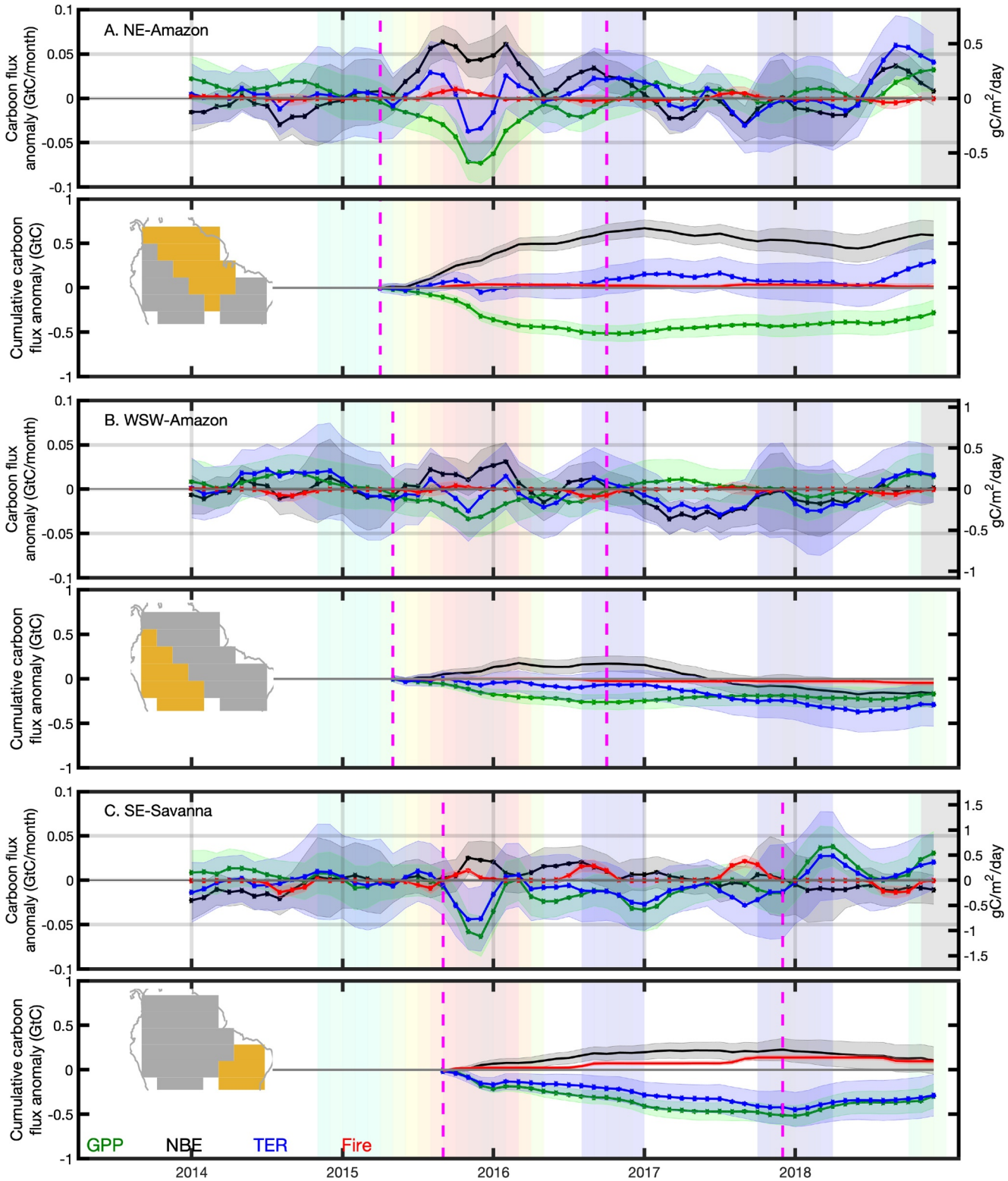

Figure 2.

3.2. The Dominant Role of the Increased Sensitivities of Carbon Fluxes to Extreme Climate Anomalies in the Response to the 2015–2016 Drought and Recovery

The recovery of the carbon cycle from the drought is in part a function of the climate forcing along with the initial carbon and hydrological state (Bloom et al., 2020). However, as this climate forcing becomes more extreme, the coupling between these processes could change (Brando et al., 2019; Frank et al., 2015; Fu et al., 2020). To quantify the contributions of changing carbon-climate sensitivities to the drought response and recovery, we first calculate carbon-climate sensitivities by linear regression of carbon flux anomalies against climate driver anomalies at three stages of drought (i.e., pre-drought, drought, and post-drought). With a stepwise multi-variable linear regression, we found that VPD anomalies (ΔVPD) explain most of the inter-annual variability (IAV) in GPP anomalies (ΔGPP). The relationship between Δ GPP and temperature anomalies are not significant ($p > 0.05$) given constant VPD during pre-drought and drought in all three regions, as reflected in the small changes in R^2 when we add temperature anomalies in the linear regression (Figure S3 in Supporting Information S1).

We therefore focus on changes in the sensitivities of ΔC to ΔVPD and the reference carbon flux anomalies from changes in water storage anomalies derived from the univariate linear regressions over these three periods (denoted as $\gamma^{c}_{\mathrm{VPD}}$). This allows us to discuss the synergistic effect between atmosphere aridity and water storage deficit at different drought stages. We quantify the impact of the changes in carbon-climate sensitivities on carbon flux anomalies by calculating what the carbon flux anomalies would be during the drought and recovery period using pre-drought $\gamma^{c}_{\mathrm{VPD}}$, which we denote as flux anomalies under "*nominal*" sensitivity (Figure 1). We then calculate the contributions from changing $\gamma^{c}_{\mathrm{VPD}}$, which we denote as anomalies under "*perturbed*" sensitivity, as the differences between flux anomalies under "*drought*" or "*post-drought*" sensitivity and the carbon flux anomalies under "*nominal*" sensitivity (Equations 6 and 9). The either enhanced or reduced response to climate anomalies is reflected in the non-zero values in the "*perturbed*" anomalies. The differences between the actual carbon flux anomalies and the sum of "*nominal*" and "*perturbed*" anomalies are residuals that could not be explained by the carbon-climate sensitivity function we fit. We primarily focus on the changes of $\gamma^{\mathrm{GPP}}_{\mathrm{VPD}}$ relationships and its contribution to ΔGPP since it is the dominant driver for the NBE anomalies during drought conditions. Because total ecosystem respiration is less sensitive to ΔVPD, the quantity $\gamma^{\mathrm{TER}}_{\mathrm{VPD}}$ (Table 1) is less robust than $\gamma^{\mathrm{GPP}}_{\mathrm{VPD}}$.

3.2.1. The Dependence of $\Delta C/\Delta\mathrm{VPD}$ ($\gamma^{c}_{\mathrm{VPD}}$) Sensitivities on the Magnitude of Climate Anomalies

The $\gamma^{\mathrm{GPP}}_{\mathrm{VPD}}$ and $\gamma^{\mathrm{NBE}}_{\mathrm{VPD}}$ show a strong regional dependence on drought stage (Figures 3a–3c and Table 1). Among the three regions, we find that ΔGPP has the largest sensitivity to ΔVPD over SE-Savanna during all three stages (Figure 3 and Table 1), corresponding to the lowest WUE and the driest climate (Table S1 in Supporting Information S1). The comparatively low WUE over SE-Savanna is consistent with previous studies (Tang et al., 2014). Persistent dryness caused by the 2015–2016 El Niño increased the absolute $\gamma^{\mathrm{GPP}}_{\mathrm{VPD}}$ over the forest, particularly a large reduction of the reference carbon flux anomalies but decreased the $\gamma^{\mathrm{GPP}}_{\mathrm{VPD}}$ over SE-Savanna (Figure 3 and Table 1).

When controlling temperature changes in calculating the partial correlation between ΔGPP and ΔVPD, the R^2 (GPP, VPD|T) is comparable with R^2 (GPP, VPD). This implies that changes in atmospheric water vapor are more important than changes in atmospheric temperature in explaining changes in atmospheric aridity and subsequently its control on GPP variability (Table 1). The increased absolute ΔGPP − ΔVPD sensitivity contributed to the increased ΔNBE − ΔVPD sensitivities during drought over the two forest regions (Figure 3).

Figure 2. The impact of the 2015–2016 drought and recovery on tropical South America (SA) biosphere carbon cycle. (a) Northeast Amazon (NE-Amazon); (b) West and southwest Amazon (WSW-Amazon); (c) Southeast-Savanna (SE-Savanna). Green, black, blue, and red are GPP, NBE, TER, and fire and the corresponding uncertainties. The top panels on (a–c) are monthly flux anomaly (GtC/month: left *y*-axis, and gC/m^2/day: right-axis). The bottom panels on (a–c) are cumulative carbon flux anomalies (GtC). The two magenta dashed lines enclose the 2015–2016 drought time period for each region. The drought period is defined from an impact perspective, corresponding to negative GPP anomalies (Section 2). The mean states are defined over January 2010–December 2018. The green to red shaded color indicates that Nino 3.4 larger than 0.5°C with increasing magnitude, while blue shaded color indicates Nino 3.4 less than −0.5°C. GPP: gross primary production; NBE: net biosphere exchange; TER: total ecosystem respiration. Even though monthly NBE and GPP have returned to pre-drought values in early to late 2017, the accumulated carbon loss represented by the accumulated NBE has not recovered in the tropical SA, dominated to the large carbon loss over NE-Amazon.

Table 1
Summary of the Linear Fitting Between Carbon Flux Anomalies (i.e., GPP and NBE) and VPD Anomalies During Pre-Drought, Drought, and Post Drought Over NE-Amazon, WSW-Amazon, and SE-Savanna Shown in Figure 3

Region	Variables	Drought stage	Slope	Intercept	R^2	*P*-value	R^2 ($\gamma_{VPD|T}$)	$P_{VPD|T}$
NE-Amazon	γ_{VPD}^{GPP}	Pre-drought	−0.14 ± 0.05	0.06 ± 0.02	0.42	<0.05	0.41	<0.05
		Drought	−0.15 ± 0.04	−0.10 ± 0.04	0.75	<0.05	0.56	<0.05
		Post-drought	−0.05 ± 0.06	0.06 ± 0.03	0.11	>0.05	0.08	>0.05
	γ_{VPD}^{NBE}	Pre-drought	0.08 ± 0.06	−0.09 ± 0.03	0.12	<0.05	0.01	>0.05
		Drought	0.10 ± 0.05	0.19 ± 0.07	0.38	<0.05	0.16	>0.05
		Post-drought	−0.14 ± 0.10	−0.03 ± 0.05	0.18	<0.05	0.29	<0.05
WSW-Amazon	γ_{VPD}^{GPP}	Pre-drought	−0.11 ± 0.04	0.07 ± 0.02	0.41	<0.05	0.34	<0.05
		Drought	−0.10 ± 0.04	−0.12 ± 0.03	0.61	<0.05	0.51	<0.05
		Post-drought	−0.07 ± 0.06	0.03 ± 0.01	0.18	<0.05	0.49	<0.05
	γ_{VPD}^{NBE}	Pre-drought	0.08 ± 0.07	0.03 ± 0.04	0.08	>0.05	0.03	>0.05
		Drought	0.10 ± 0.07	0.07 ± 0.05	0.24	<0.05	0.00	>0.05
		Post-drought	−0.17 ± 0.07	−0.15 ± 0.03	0.40	<0.05	0.12	>0.05
SE-Savanna	γ_{VPD}^{GPP}	Pre-drought	−0.36 ± 0.06	−0.11 ± 0.04	0.73	<0.05	0.62	<0.05
		Drought	−0.20 ± 0.08	−0.18 ± 0.10	0.40	<0.05	0.23	<0.05
		Post-drought	−0.43 ± 0.13	0.07 ± 0.09	0.62	<0.05	0.66	<0.05
	γ_{VPD}^{NBE}	Pre-drought	0.13 ± 0.06	−0.04 ± 0.04	0.25	<0.05	0.04	>0.05
		Drought	0.10 ± 0.05	0.09 ± 0.05	0.37	<0.05	0.01	>0.05
		Post-drought	0.02 ± 0.0.4	−0.15 ± 0.03	0.08	>0.05	0.01	>0.05

Note. γ_{VPD}^{GPP} represents the linear fitting between GPP anomalies and VPD anomalies, while γ_{VPD}^{NBE} represents the linear fitting between NBE anomalies and VPD anomalies. The table also shows R^2 ($\gamma_{VPD|T}$) and $P_{VPD|T}$ values for the partial linear regression between carbon flux anomalies and VPD when controlling temperature changes.

The changes in the sensitivities of carbon fluxes to climate anomalies and reference values during the drought stage are also observed in the ΔNIRv/ΔVPD and ΔSIF/ΔVPD relationships over the forest regions (Figures S4 and S5 in Supporting Information S1), supporting the reduction of photosynthesis due to reduction of water storage and changes in the sensitivity to ΔVPD with persistent drought. The increasing sensitivity of photosynthesis to VPD anomalies as the soil water decreases was previously observed in field-grown crops (Xue et al., 2004).

During the recovery stage, the ΔGPP/ΔVPD relationships became less significant ($p > 0.05$) over both forest regions, suggesting a lagged effect from the 2015–2016 drought (Bloom et al., 2020; Frank et al., 2015), while over SE-Savanna the absolute ΔGPP/ΔVP relationships became larger and more significant. The differences in the γ_{VPD}^{GPP} over the three regions during the recovery stage is consistent with differences in the ΔSIF/ΔVPD and ΔNIRv/ΔVPD relationships (Figures S4 and S5 in Supporting Information S1).

The increased ΔGPP/ΔVPD sensitivity during persistent drought is further supported by flux tower observations. Within the LBA-ECO flux tower network (Saleska et al., 2013), we find the BR-Sa3 site (see Section 2), located within the NE-Amazon region (3.02 S, 54.98 W), experienced a drought event longer than 12 months (Figure S6 in Supporting Information S1). While there was essentially no sensitivity of ΔGPP to ΔVPD during non-drought conditions, the relationship became highly negative during drought (Figure S6 in Supporting Information S1).

3.2.2. The Contributions of the Changing Sensitivities of Carbon Flux Anomalies to Extreme Climate Anomalies in the Response to the 2015–2016 Drought and Recovery

The shift in γ_{VPD}^{GPP} from pre-drought to drought was the major driver for the GPP reduction during drought in two forest regions. If γ_{VPD}^{GPP} had remained unchanged, the GPP reduction would have been only about 20% of the actual GPP reduction over NE-Amazon during the drought (0.11 ± 0.06 vs. 0.51 ± 0.16 GtC; light blue relative to brown in Figure 4a; Table S4 in Supporting Information S1), and over the WSW-Amazon, the GPP would have increased by 0.06 ± 0.04 GtC instead of decreasing by 0.26 ± 0.11 GtC (Figure 4b and Table S4 in Supporting

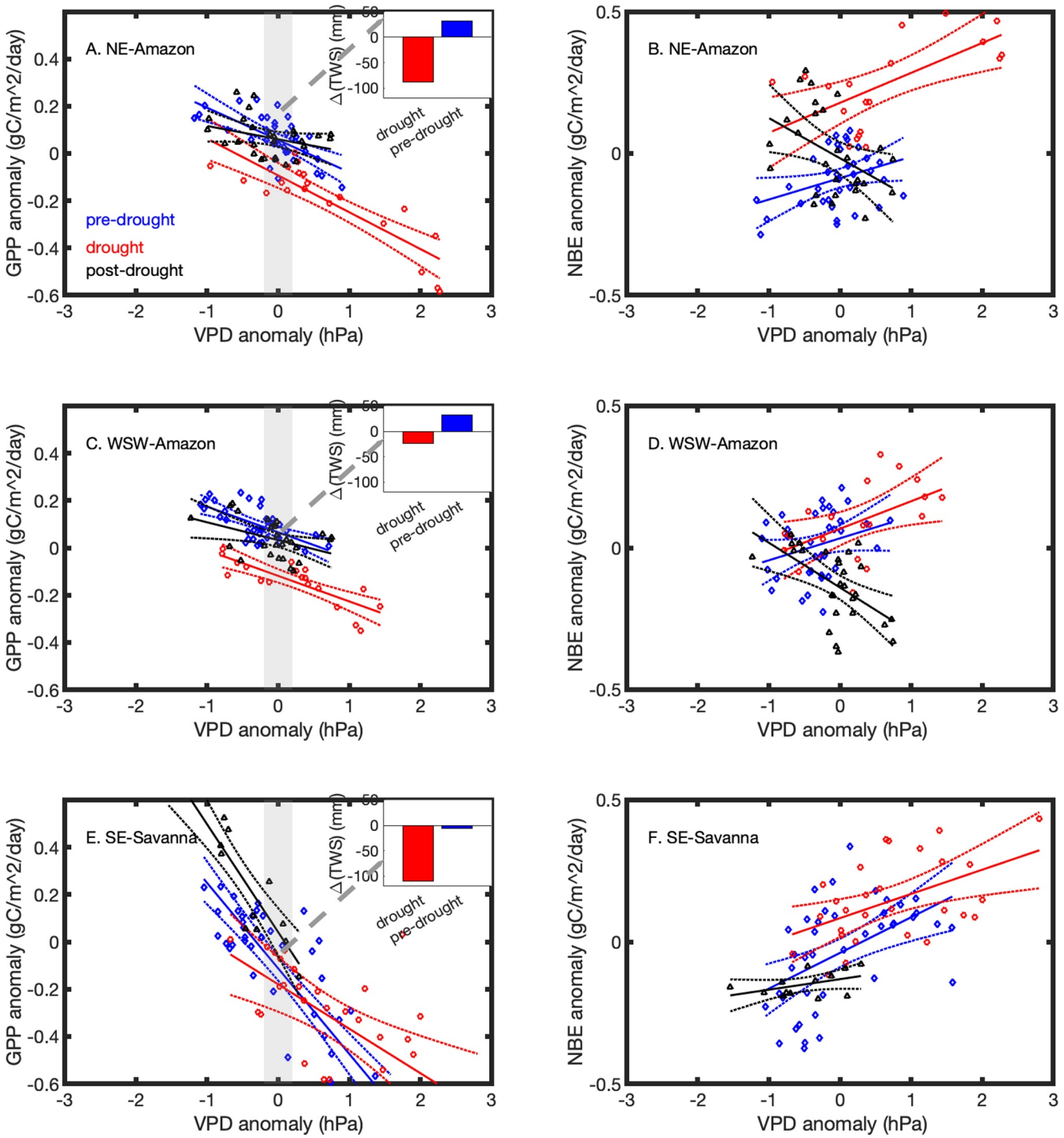

Figure 3. Sensitivities of carbon flux anomalies to VPD during pre-drought (blue), drought (red), and post-drought (black) conditions, 2015–2016. Left panels: Regional scatterplots of GPP or NBE anomaly and VPD anomaly for NE Amazon (a) and (b), WSW Amazon (c) and (d), and SE-Savanna (e) and (f) (regions are defined in Figure 1). Linear model fits of carbon flux anomalies and VPD anomalies during pre-drought, drought, and post-drought conditions are denoted by blue, red, and black lines, respectively; linear fit parameters are reported in Table 1. Inset plots on left three panels show the TWS anomaly during drought (red) and pre-drought (blue) conditions when the absolute VPD anomaly is less than 0.2 hPa (denoted by gray shaded area and the gray arrows indicate where the TWS anomalies were calculated). The sensitivity of carbon flux anomalies to atmosphere aridity greatly increased during drought and decreased post drought compared to pre-drought over the two forest regions, reflected in the changes in both the slope and the intercept, while the sensitivity of GPP to atmosphere aridity changed in the opposite direction over SE-Savanna.

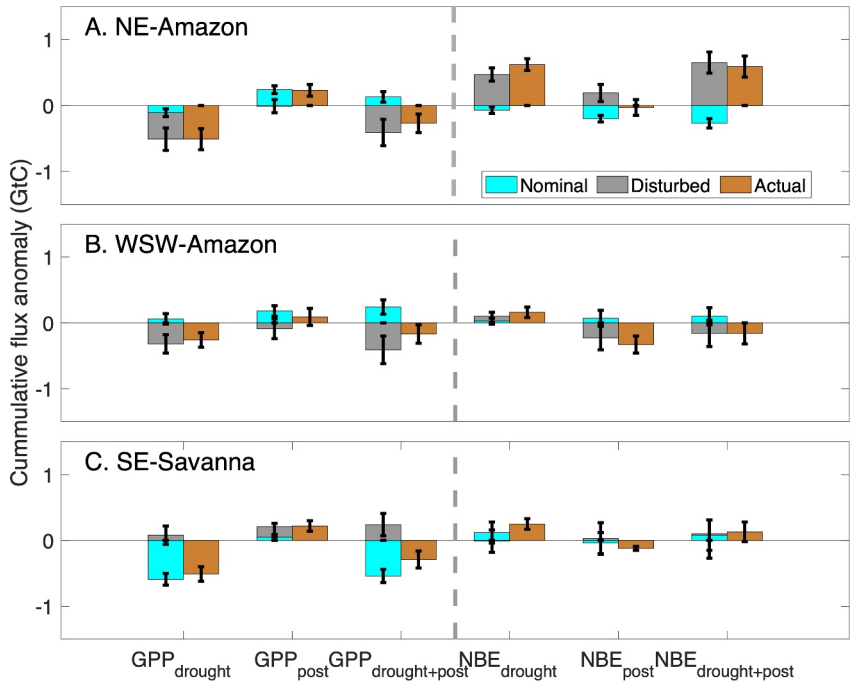

Figure 4. The enhanced response to atmosphere aridity greatly increased the carbon loss during drought and slowed the recovery afterward. Light blue: the carbon flux anomalies based on pre-drought (*nominal*) sensitivities to atmosphere aridity; Gray: the carbon flux anomalies attributed to changing sensitivities (*disturbed*) to atmosphere aridity; Brown: the actual cumulative carbon flux anomalies (*actual*) during drought and post drought. The carbon flux anomalies based on either the drought or post-drought sensitivities to atmosphere aridity are the sum of nominal anomalies (light blue) and the disturbed anomalies. The difference between the brown bars and the sum of light blue and gray color represents the residual carbon flux anomalies that cannot be explained by the sensitivities to atmosphere aridity. (a) NE-Amazon; (b) WSW-Amazon; (c) SE-Savanna. Over SE-Savanna, the changing sensitivity during drought has less impact on GPP than on NBE.

Information S1). Of the 0.51 ± 0.16 GtC GPP reduction over NE-Amazon, −0.26 ± 0.08 GtC anomalies come from the VPD anomalies ($\Delta GPP^{slope}_{drought}$ in Table S4 of the Supporting Information S1), and −0.25 ± 0.13 GtC comes from reference carbon flux anomalies due to the water storage deficit during drought (Table S4 in Supporting Information S1). The reference ΔGPP is 0.13 ± 0.03 under the pre-drought state, (Table S4 in Supporting Information S1), implying the strong impact of the changes in water storage during drought on plants productivity. Over the WSW-Amazon, change of the reference carbon flux anomalies is also the main contributor to the changes in γ^{GPP}_{VPD} (Table S4 in Supporting Information S1). Different from the two forest regions, over SE-Savanna, the change in γ^{GPP}_{VPD} reduced the drought impact on GPP by 0.08 ± 0.14 GtC (Figure 4c and Table S4 in Supporting Information S1).

During the post-drought, the perturbation in γ^{GPP}_{VPD} (gray bars in Figure 4) slowed the GPP recovery by 50% over the WSW-Amazon but accelerated the GPP recovery over savanna/shrubland (Figure 4c and Table S4 in Supporting Information S1). Over the whole drought and post-drought period, the GPP would have increased by 0.37 ± 0.14 GtC over the NE-Amazon and WSW-Amazon by December 2018 based on the nominal γ^{GPP}_{VPD} (light blue in Figure 4), instead of decreasing by 0.45 ± 0.25 GtC (brown in Figure 4). The enhanced sensitivity to atmospheric aridity and changes in reference carbon flux anomalies due to water storage anomalies during the drought exacerbated the reduction in GPP and therefore slowed the recovery over these two forest regions. While over SE-Savanna, the GPP would have decreased by 0.53 ± 0.74 GtC under pre-drought sensitivity instead of decreasing only by 0.29 ± 0.14 GtC by December 2018. Thus, the savanna/shrubland is more resilient to drought (Stuart-haëntjens et al., 2018).

The increased coupling between NBE and atmospheric aridity during the drought leads to much larger NBE responses over all three regions (Figure 4 and Table S4 in Supporting Information S1). The changes in reference carbon flux anomalies from changes in water availability during drought contributed an additional

0.46 ± 0.12 GtC released to the atmosphere primarily over NE-Amazon (Table S4 in Supporting Information S1), about 74% of the actual NBE anomaly. Over SE-Savanna, despite the reduced GPP response to VPD anomalies, the change in γ_{VPD}^{NBE} increased NBE anomalies by 0.13 ± 0.08 GtC because of the increased sensitivity of the TER anomaly to ΔVPD (Figure S7 in Supporting Information S1). During post-drought recovery, the cumulative net carbon uptake anomaly was close to zero over NE-Amazon (NBE_{post}; Figure 4a). Under the nominal sensitivity, the carbon uptake would have been −0.20 ± 0.05 GtC. However, the changed γ_{VPD}^{NBE} led to a substantial increase in carbon loss of 0.20 ± 0.13 GtC leading to a neutral accumulation. Consequently, the loss of carbon during the drought was not compensated by an expected post-drought recovery. Over the WSW-Amazon, however, the −0.33 ± 0.13 GtC cumulative net carbon uptake anomaly largely originated from the change in ΔTER/ΔVPD sensitivity (Figure S7 in Supporting Information S1), driven by decreased TER. Reduced TER during post-drought periods over the Amazon has also been observed in plot data during previous droughts, caused by changes in carbon allocation strategies during drought (Doughty et al., 2015). Reduced TER has also been observed during post-fire recovery (Brando et al., 2019). Thus, over the WSW-Amazon, even with the muted GPP recovery, possibly due to lagged effects on TER from the drought, NBE still showed the strongest recovery rate. Overall, however, the change in γ_{VPD}^{NBE} during drought and recovery resulted in an additional 0.53 ± 0.38 GtC released to atmosphere over tropical SA, which is comparable to the actual 0.65 ± 0.28 GtC cumulative NBE anomaly by December 2018. This suggests that the tropical SA carbon cycle would have largely recovered from drought by December 2018 based upon nominal sensitivities to ΔVPD and pre-drought reference carbon flux anomaly state during the drought and recovery periods.

3.2.3. What Causes the Δ*C*/ΔVPD Sensitivities to Change During Drought?

We explore the possible mechanisms causing the changes in ΔC/ΔVPD sensitivities (γ_{VPD}^{C}) during persistent drought conditions from two intrinsically linked perspectives: adaptation strategies unique to vegetation types and climate and the coupling between water supply and atmospheric water demand.

The WSW-Amazon includes the wettest part of Amazon with a short dry season (Carvalho et al., 2021) and annual mean precipitation larger than 2000 mm/year (Table S1 in Supporting Information S1). The normal ample water supply causes the transpiration to be atmospheric demand-limited even during drought (Y. N. Pokhrel et al., 2014). Thus, in response to a large increase in VPD, both transpiration and total evapotranspiration (ET) increased despite decreasing GPP (Figure S8 in Supporting Information S1). As a result, WUE decreases (Table S4 in Supporting Information S1). The increase of evapotranspiration coupled with decreasing precipitation reduced soil water content during drought. Even with climatological values of VPD (i.e., VPD anomaly is within 0.2 hPa), the TWS anomaly (ΔTWS) declined by 55.1 mm over WSW-Amazon from pre-drought to drought, contributing to the changes in reference carbon flux anomalies in γ_{VPD}^{C} (Figure 3 and Table 1). The coupling effect between ΔVPD and ΔTWS in controlling GPP variability is supported by the increased R^2 from 0.66 to 0.76 when including the interactive effect between ΔVPD and ΔTWS in the multi-variable linear regression (Figure S3 in Supporting Information S1). Reduced water supply and increased water demand from increasing VPD can cause failure in hydraulic transport and subsequent mortality (da Costa et al., 2010; Olson et al., 2018), which is especially prevalent in large trees during persistent drought (da Costa et al., 2010) and may have contributed the decrease in GPP. The legacy effect of hydraulic failure during drought could also contribute to the slow recovery of WUE and GPP (Bennett et al., 2023; Brodribb & Cochard, 2009).

Compared to the WSW-Amazon, the forest over the NE-Amazon has less annual precipitation and has experienced much larger reduction in ground water during drought (Figure S2 in Supporting Information S1). During the drought stage, TWS declined by 120.1 mm from pre-drought under the climatological VPD value, driving the large change in the reference carbon flux anomalies from pre-drought to drought for both GPP and NBE (Figure 3 and Table S4 in Supporting Information S1). As a result, despite the relatively small changes in transpiration during early drought, the large reduction of water supply causes the transpiration to become water-supply limited. Thus, transpiration decreases as the drought persists (Figure S2 in Supporting Information S1). The reduction in ET and TWS under high VPD condition indicates that water demand is not being met and suggest that there is considerable water stress occurring, consistent with the greatly decreased GPP. The synchronization of decrease in both ET and GPP leads to much smaller changes in WUE compared to the WSW-Amazon (Table S4 and Figure S8 in Supporting Information S1). Consistent with being more drought tolerant, the WUE and GPP quickly recovered after drought in the NE-Amazon (Table S4 in Supporting Information S1).

The increased sensitivity of the carbon cycle to the intense atmospheric aridity during a loss of soil water supply is confirmed with the observations from the BR-Sa3 site. Due to the persistent drought at the site, the soil water content reduced; the rate in soil moisture anomaly decreased from +3.4 mm/month during pre-drought to −5.4 mm/month during the drought when the absolute VPD anomaly was within 0.3 hPa, implying the combined effect of reduced soil water supply and increased atmospheric aridity led to changes in the ΔGPP/ΔVPD sensitivities (Figure S6 in Supporting Information S1). The large reduction of water storage was also observed in other field experiments (Jipp et al., 1998).

The SE-Savanna is most adapted to drought stress. During the drought period, the transpiration rate decreased the most while WUE remained comparable to the value during the pre-drought period (Table S4 in Supporting Information S1), and the land-atmosphere coupling weakened (Figure S9 in Supporting Information S1) that resulted in reduced absolute ΔGPP/ΔVPD sensitivity (Figure S10 in Supporting Information S1). The land-atmosphere coupling recovered to pre-drought level (Figure S9 in Supporting Information S1) and WUE quickly recovered to the above-normal value after drought, which led to the overshooting GPP recovery (Table S4 in Supporting Information S1).

4. Discussion

The relative resistance and resilience to drought among the three regions revealed in this study is consistent with the resistance-resilience theory and the meta-analysis based on flux tower observations in Stuart-Haëntjens et al. (2018), that suggests that wetter forests are generally more resistant to drought but take longer to recover (i.e., less resilient). By contrast, dry forest and savanna/shrubland ecosystems are less resistant to drought due to lower soil moisture but recover faster due to more rapid recovery of grasses and sprouting shrubs.

The SE-Savanna ecosystem showed less resistance to drought—ΔGPP has the largest sensitivity to ΔVPD (Table 1)—but more resilience, reflected in the much stronger GPP recovery, than predicted by the pre-drought ΔGPP/ΔVPD sensitivity (Figure 4). In the SE-Savanna, the plants quickly reduced water loss during drought, preventing structural damage to the plants and ensuring a quick recovery. Similarly strong post-drought recovery of savanna/shrubland is reported in field experiments over Africa (Wilcox et al., 2020). Additionally, it takes time to recharge soils. This time frame may be shorter for shrublands because they have lower foliage cover and have less water demand (Ivanov et al., 2012; Longo et al., 2018).

In contrast, the continued water loss over WSW-Amazon during drought may have caused functional impairment (e.g., lost xylem hydraulic conductance) and damage to sensitive plant species (Ruehr et al., 2019), which contributes to the slow recovery of GPP after drought. The long-term throughfall exclusion experiment observed higher percentage of mortality from larger trees as drought persists, supporting our hypothesis (da Costa et al., 2010). Any impact of tree mortality on soil carbon pools and the subsequent soil respiration have been accounted for in the NBE anomalies. Nonetheless, more observations are needed to better understand the couplings among water loss, plant functional changes, and drought recovery.

The response of GPP and TER to the 2015–2016 drought and recovery was asynchronous in time over the forest regions: the GPP anomaly was the dominant driver for the NBE increase during the drought, but TER played a much larger role following the event. We attribute the much larger increase of net carbon uptake during post-drought over the WSW-Amazon to the decrease of TER. Considering only the slow recovery of GPP, the carbon sink would have declined, consistent with a weakened carbon sink after drought based on above-ground biomass over Amazonia forest (Yang et al., 2018). Even though reduced TER after drought was observed in forest plots in previous drought (Doughty et al., 2015) and in controlled fire experiment (Brando et al., 2019), more in situ measurements are needed to test our conclusion. In the SE-Savanna, however, responses were more synchronous, reflected in the reduction in both GPP and TER during drought and an increase of both GPP and TER afterward. This phase difference between GPP and TER response over the forest and savanna/shrubland may be due to the longer residence time of foliage and fine roots over forest than over savanna/shrubland (Bloom et al., 2016).

The CMIP6 models predict a reduction of total water storage (TWS) by 50–200 mm over Amazon under RCP 6.0 scenario by the late 21st century, especially over the NE-Amazon and southwest Amazon (Jensen et al., 2020; Y. Pokhrel et al., 2021)—an anomaly larger than the TWS anomaly seen during 2015–2016 El Niño over some regions. Our results suggest that both GPP and net carbon uptake will become more sensitive to atmospheric aridity over the Amazon with the decrease of TWS in the future, making the terrestrial carbon cycle more

vulnerable to drought. As a result, tropical SA may become a source of carbon to the atmosphere due to increasing drought events and decreasing TWS in the future instead of the current net carbon-neutral state (Liu et al., 2020) (i.e., carbon uptake is of a similar magnitude to carbon release). Recent results from Gatti et al. (2021) suggest that this shift of sink to source may already be occurring in the highly degraded forests in the Southeastern Amazon. Currently, the biosphere on land absorbs about a quarter of fossil fuel emissions annually, a weakening of this uptake increases the pressure to increase the rate of reducing fossil fuel emissions and develop other negative emissions technologies to limit the temperature increase to 2.0°C by the end of this century.

5. Conclusion

We find that the carbon loss due to the 2015–2016 drought had not fully recovered by the end of 2018 over the tropical South America, driven by a persistent carbon loss in the Northeast Amazon. We attribute the slow recovery to the large carbon loss from the intense atmospheric aridity, coupled with changes of reference carbon flux anomalies due to reduced water supply during drought. Our results suggest that the tropical south America carbon cycle would have largely recovered from drought by December 2018 based upon nominal sensitivities to ΔVPD and pre-drought reference carbon flux anomaly state during the drought and recovery periods. We show that the attenuation of carbon uptake is three times higher than expected from the pre-drought sensitivity to atmospheric aridity and ground water supply. Our study provides empirical evidence for the enhanced response of forests to compound anomalies in atmospheric aridity and total water storage anomalies during severe drought (Breshears et al., 2013). The increased sensitivity to atmospheric aridity during drought was concurrent with the strengthening of the land-atmosphere coupling, highlighting the importance of accurately simulating land-atmosphere interactions in earth system models (Humphrey et al., 2021).

Conflict of Interest

The authors declare no conflicts of interest relevant to this study.

Data Availability Statement

(1) CMS-Flux NBE 2020 is available at: https://cmsflux.jpl.nasa.gov/get-data/nbe-2020/ (Liu et al., 2020).
(2) GEOS-Chem-EnKF NBE is available at: https://www.nceo.ac.uk/data-tools/atmospheric-tools/.
(3) FluxSAT GPP is available at: https://gs614-avdc1-pz.gsfc.nasa.gov/pub/tmp/FluxSat_GPP/.
(4) MODIS NIRv is available at https://modis.gsfc.nasa.gov/data/dataprod/.
(5) OCO-2 SIF B10 is available at: https://disc.sci.gsfc.nasa.gov/datasets/OCO2_L2_Lite_SIF_10r/summary?keywords=OCO2%20L2%20SIF%20lite (Kiel et al., 2019).
(6) ERA5 VPD is available at https://cds.climate.copernicus.eu/cdsapp#!/dataset/reanalysis-era5-land-monthly-means?tab=overview (Muñoz Sabater, J., 2019).
(7) GRACE TWS is available at: https://grace.jpl.nasa.gov/data/get-data/.
(8) GLEAM evapotranspiration and transpiration is available at https://www.gleam.eu/.
(9) Nino 3.4 index is available at: https://climatedataguide.ucar.edu/climate-data/nino-sst-indices-nino-12-3-34-4-oni-and-tni (Schneider et al., 2013).
(10) LBA-ECO CD-32 Flux Tower Network Data Compilation is available at https://doi.org/10.3334/ORNLDAAC/1174 (Saleska et al., 2013).

Acknowledgments
National Aeronautics and Space Administration Interdisciplinary Research in Earth Science (JL, KB, SS, MK, PL, AAB), National Aeronautics and Space Administration Orbiting Carbon Observatory Science Team program and Carbon Cycle Science program (JL), National Aeronautics and Space Administration postdoc program (ML), Department of Energy Next Generation Ecosystem Experiments-Tropics fund (ML), National Centre for Earth Observation funded by the National Environment Research Council (NE/R016518/1) (PIP and LF). Part of the research was carried out at the Jet Propulsion Laboratory, California Institute of Technology, under a contract with the National Aeronautics and Space Administration, (80NM0018D0004).

References

Badgley, G., Field, C. B., & Berry, J. A. (2017). Canopy near-infrared reflectance and terrestrial photosynthesis. *Science Advances*, *3*(3), e1602244. https://doi.org/10.1126/sciadv.1602244

Baker, J. C. A., Buermann, W., Castilho De Souza, D., Marsham, J. H., Kubota, P. Y., Gloor, M., et al. (2021). Robust Amazon precipitation projections in climate models that capture realistic land—Atmosphere interactions OPEN ACCESS robust Amazon precipitation projections in climate models that capture realistic land—Atmosphere interactions. *Environmental Research Letters*, *16*(7), 074002. https://doi.org/10.1088/1748-9326/abfb2e

Barkhordarian, A., Bowman, K. W., Cressie, N., Jewell, J., & Liu, J. (2021). Emergent constraints on tropical atmospheric aridity–carbon feedbacks and the future of carbon sequestration. *Environmental Research Letters*, *16*(11), 114008. https://doi.org/10.1088/1748-9326/ac2ce8

Barkhordarian, A., Saatchi, S. S., Ali, B., Loikith, P. C., & Mechoso, C. R. (2019). OPEN a recent systematic increase in vapor pressure deficit over tropical South America (pp. 1–12). https://doi.org/10.1038/s41598-019-51857-8

Bennett, A. C., Rodrigues de Sousa, T., Monteagudo-Mendoza, A., Esquivel-Muelbert, A., Morandi, P. S., Coelho de Souza, F., et al. (2023). Sensitivity of South American tropical forests to an extreme climate anomaly. *Nature Climate Change*, *13*(9), 967–974. https://doi.org/10.1038/s41558-023-01776-4

Bloom, A. A., Bowman, K. W., Liu, J., Konings, A. G., Worden, J. R., Parazoo, N. C., et al. (2020). Lagged effects regulate the inter-annual variability of the tropical carbon balance. *Biogeosciences*, *17*(24), 6393–6422. https://doi.org/10.5194/bg-17-6393-2020

Bloom, A. A., Exbrayat, J.-F., van der Velde, I. R., Feng, L., & Williams, M. (2016). The decadal state of the terrestrial carbon cycle: Global retrievals of terrestrial carbon allocation, pools, and residence times. *Proceedings of the National Academy of Sciences of the United States of America*, *113*(5), 1285–1290. https://doi.org/10.1073/pnas.1515160113

Bonal, D., Burban, B., Stahl, C., Wagner, F., & Hérault, B. (2016). The response of tropical rainforests to drought—Lessons from recent research and future prospects. *Annals of Forest Science*, *73*(1), 27–44. https://doi.org/10.1007/s13595-015-0522-5

Bonan, G. B., Lombardozzi, D. L., Wieder, W. R., Oleson, K. W., Lawrence, D. M., Hoffman, F. M., & Collier, N. (2019). Model structure and climate data uncertainty in historical simulations of the terrestrial carbon cycle (1850–2014). *Global Biogeochemical Cycles*, *33*(10), 1310–1326. https://doi.org/10.1029/2019GB006175

Bowman, K. W., Liu, J., Bloom, A. A., Parazoo, N. C., Lee, M., Jiang, Z., et al. (2017). Global and Brazilian carbon response to El Niño Modoki 2011–2010. *Earth and Space Science*, *4*(10), 637–660. https://doi.org/10.1002/2016EA000204

Brando, P. M., Silvério, D., Maracahipes-Santos, L., Oliveira-Santos, C., Levick, S. R., Coe, M. T., et al. (2019). Prolonged tropical forest degradation due to compounding disturbances: Implications for CO_2 and H_2O fluxes. *Global Change Biology*, *25*(9), 2855–2868. https://doi.org/10.1111/gcb.14659

Breshears, D., Adams, H., Eamus, D., McDowell, N., Law, D., Will, R., et al. (2013). The critical amplifying role of increasing atmospheric moisture demand on tree mortality and associated regional die-off. *Frontiers in Plant Science*, *4*. https://doi.org/10.3389/fpls.2013.00266

Brodribb, T. J., & Cochard, H. (2009). Hydraulic failure defines the recovery and point of death in water-stressed conifers. *Plant Physiology*, *149*(1), 575–584. https://doi.org/10.1104/pp.108.129783

Carvalho, N. S., Anderson, L. O., Nunes, C. A., Pessôa, A. C. M., Silva Junior, C. H. L., Reis, J. B. C., et al. (2021). Spatio-temporal variation in dry season determines the Amazonian fire calendar. *Environmental Research Letters*, *16*(12), 125009. https://doi.org/10.1088/1748-9326/ac3aa3

Cook, B. I., Mankin, J. S., Marvel, K., Williams, A. P., Smerdon, J. E., & Anchukaitis, K. J. (2019). Twenty-first century drought projections in the CMIP6 forcing scenarios. *Earth's Future*, *8*(6), 1–20. https://doi.org/10.1029/2019EF001461

da Costa, A. C. L., Galbraith, D., Almeida, S., Portela, B. T. T., da Costa, M., de Silva Junior, J. A., et al. (2010). Effect of 7 Yr of experimental drought on vegetation dynamics and biomass storage of an eastern Amazonian rainforest. *New Phytologist*, *187*(3), 579–591. https://doi.org/10.1111/j.1469-8137.2010.03309.x

Deeter, M. N. (2018). Satellite-based analysis of CO seasonal and interannual (pp. 5641–5656).

Doughty, C. E., Metcalfe, D. B., Girardin, C. A. J., Amézquita, F. F., Cabrera, D. G., Huaraca Huasco, W., et al. (2015). Drought impact on forest carbon dynamics and fluxes in Amazonia. *Nature*, *519*(7541), 78–82. https://doi.org/10.1038/nature14213

Feng, L., Palmer, P. I., Bösch, H., & Dance, S. (2009). Estimating surface CO_2 fluxes from space-borne CO_2 dry air mole fraction observations using an ensemble Kalman filter. *Atmospheric Chemistry and Physics*, *9*(8), 2619–2633. https://doi.org/10.5194/acp-9-2619-2009

Frank, D., Reichstein, M., Bahn, M., Thonicke, K., Frank, D., Mahecha, M. D., et al. (2015). Effects of climate extremes on the terrestrial carbon cycle: Concepts, processes and potential future impacts. *Global Change Biology*, *21*(8), 2861–2880. https://doi.org/10.1111/gcb.12916

Frankenberg, C., Fisher, J. B., Worden, J., Badgley, G., Saatchi, S. S., Lee, J.-E., et al. (2011). New global observations of the terrestrial carbon cycle from GOSAT: Patterns of plant fluorescence with gross primary productivity. *Geophysical Research Letters*, *38*(17), L17706. https://doi.org/10.1029/2011GL048738

Fu, Z., Ciais, P., Bastos, A., Stoy, P. C., Yang, H., Green, J. K., et al. (2020). Sensitivity of gross primary productivity to climatic drivers during the summer drought of 2018 in Europe. *Philosophical Transactions of the Royal Society B: Biological Sciences*, *375*(1810), 20190747. https://doi.org/10.1098/rstb.2019.0747

Gatti, L. V., Gatti Domingues, L., Cassol, H. L. G., Tejada, G., Aragão, L. E. O. C., Corrêa, S. M., et al. (2021). Amazonia as a carbon source linked to deforestation and climate change. *Nature*, *595*(7867), 388–393. https://doi.org/10.1038/s41586-021-03629-6

Grossiord, C., Grossiord, C., Buckley, T. N., Cernusak, L. A., Novick, K. A., Poulter, B., et al. (2020). Tansley review plant responses to rising vapor pressure deficit (pp. 1550–1566). https://doi.org/10.1111/nph.16485

Harris, N. L., Gibbs, D. A., Baccini, A., Birdsey, R. A., de Bruin, S., Farina, M., et al. (2021). Global maps of twenty-first century forest carbon fluxes. *Nature Climate Change*, *11*(3), 234–240. https://doi.org/10.1038/s41558-020-00976-6

Hubau, W., Simon, L. L., Phillips, O. L., Affum-Baffoe, K., Beeckman, H., Cuní-Sanchez, A., et al. (2020). Asynchronous carbon sink saturation in African and Amazonian tropical forests. *Nature*, *579*(7797), 80–87. https://doi.org/10.1038/s41586-020-2035-0

Humphrey, V., Berg, A., Ciais, P., Gentine, P., Jung, M., Reichstein, M., et al. (2021). Soil moisture–atmosphere feedback dominates land carbon uptake variability. *Nature*, *592*(7852), 65–69. https://doi.org/10.1038/s41586-021-03325-5

Ivanov, V. Y., Hutyra, L. R., Wofsy, S. C., Munger, J. W., Saleska, S. R., de Oliveira, R. C., Jr., & de Camargo, P. B. (2012). Root Niche separation can explain avoidance of seasonal drought stress and vulnerability of overstory trees to extended drought in a mature Amazonian forest. *Water Resources Research*, *48*(12), W12507. https://doi.org/10.1029/2012WR011972

Jensen, L., Eicker, A., Dobslaw, H., & Pail, R. (2020). Emerging changes in terrestrial water storage variability as a target for future satellite gravity missions. *Remote Sensing*, *12*(23), 3898. https://doi.org/10.3390/rs12233898

Jimenez, J. C., Libonati, R., & Peres, L. F. (2018). Droughts over Amazonia in 2005, 2010, and 2015: A cloud cover perspective. *Frontiers in Earth Science*, *6*, 1–7. https://doi.org/10.3389/feart.2018.00227

Jiménez-Muñoz, J. C., Mattar, C., Barichivich, J., Santamaría-Artigas, A., Takahashi, K., Malhi, Y., et al. (2016). Record-breaking warming and extreme drought in the Amazon rainforest during the course of El Niño 2015–2016. *Scientific Reports*, *6*(1), 33130. https://doi.org/10.1038/srep33130

Jipp, P. H., Nepstad, D. C., Cassel, D. K., & Reis De Carvalho, C. (1998). Deep soil moisture storage and transpiration in forests and pastures of seasonally-dry Amazonia. *Climatic Change*, *39*(2), 395–412. https://doi.org/10.1023/A:1005308930871

Joiner, J., & Yoshida, Y. (2020). Satellite-based reflectances capture large fraction of variability in global gross primary production (GPP) at weekly time scales. *Agricultural and Forest Meteorology*, *291*, 108092. https://doi.org/10.1016/j.agrformet.2020.108092

Joiner, J., Yoshida, Y., Zhang, Y., Duveiller, G., Jung, M., Lyapustin, A., et al. (2018). Estimation of terrestrial global gross primary production (GPP) with satellite data-driven models and eddy covariance flux data. *Remote Sensing*, *10*(9), 1346. https://doi.org/10.3390/rs10091346

Kiel, M., O'Dell, C. W., Fisher, B., Eldering, A., Nassar, R., MacDonald, C. G., & Wennberg, P. O. (2019). How bias correction goes wrong: Measurement of X_{CO2} affected by erroneous surface pressure estimates [Dataset]. *Atmospheric Measurement Techniques*, *12*(4), 2241–2259. https://doi.org/10.5194/amt-12-2241-2019

Kumar, A., & Hoerling, M. P. (2003). The nature and causes for the delayed atmospheric response to El Niño. *Journal of Climate*, *16*(9), 1391–1403. https://doi.org/10.1175/1520-0442(2003)16<1391:TNACFT>2.0.CO;2

Lewis, S. L., Paulo, M. B., Oliver, L. P., van der Heijden, G. M. F., & Nepstad, D. (2011). The 2010 Amazon drought. *Science*, *331*(6017), 554LP–554. https://doi.org/10.1126/science.1200807

Liu, J., Baskaran, L., Bowman, K., Schimel, D., Bloom, A. A., Parazoo, N. C., et al. (2020). Carbon monitoring system flux net biosphere exchange 2020 (CMS-Flux NBE 2020) [Dataset]. *Earth System Science Data Discussions*, *2020*, 1–53. https://doi.org/10.5194/essd-2020-123

Liu, J., Bowman, K. W., Lee, M., Henze, D. K., Bousserez, N., Brix, H., et al. (2014). Carbon monitoring system flux estimation and attribution: Impact of ACOS-GOSAT XCO_2 sampling on the inference of terrestrial biospheric sources and sinks. *Tellus Series B Chemical and Physical Meteorology*, *66*(1), 22486. https://doi.org/10.3402/tellusb.v66.22486

Liu, J., Bowman, K. W., Schimel, D. S., Parazoo, N. C., Jiang, Z., Lee, M., et al. (2017). Contrasting carbon cycle responses of the tropical continents to the 2015–2016 El Niño. *Science*, *358*(6360). https://doi.org/10.1126/science.aam5690

Longo, M., Knox, R. G., Levine, N. M., Alves, L. F., Bonal, D., Camargo, P. B., et al. (2018). Ecosystem heterogeneity and diversity mitigate Amazon forest resilience to frequent extreme droughts. *New Phytologist*, *219*(3), 914–931. https://doi.org/10.1111/nph.15185

Martens, B., Miralles, D. G., Lievens, H., Schalie, R. V. D., & De Jeu, R. A. M. (2017). GLEAM v3: Satellite-based land evaporation and root-zone soil moisture (pp. 1903–1925). https://doi.org/10.5194/gmd-10-1903-2017

Meir, P., Brando, P. M., Nepstad, D., Vasconcelos, S., Costa, A. C. L., Davidson, E., et al. (2009). The effects of drought on Amazonian rain forests (pp. 429–449).

Melo, D. C. D., Anache, J. A. A., Borges, V. P., Miralles, D. G., Martens, B., Fisher, J. B., et al. (2021). Are remote sensing evapotranspiration models reliable across South American ecoregions? *Water Resources Research*, *57*(11), e2020WR028752. https://doi.org/10.1029/2020WR028752

Miralles, D. G., Brutsaert, W., Dolman, A. J., & Gash, J. H. (2020). On the use of the term 'evapotranspiration'. *Water Resources Research*, e2020WR028055. https://doi.org/10.1029/2020WR028055

Muñoz Sabater, J. (2019). ERA5-Land monthly averaged data from 1950 to present [Dataset]. *Copernicus Climate Change Service (C3S) Climate Data Store (CDS)*. https://doi.org/10.24381/cds.68d2bb30

Novick, K. A., Ficklin, D. L., Stoy, P. C., Williams, C. A., Bohrer, G., Christopher Oishi, A., et al. (2016). The increasing importance of atmospheric demand for ecosystem water and carbon fluxes. *Nature Climate Change*, *6*(11), 1023–1027. https://doi.org/10.1038/nclimate3114

O'Dell, C. W., Eldering, A., Wennberg, P. O., Crisp, D., Gunson, M. R., Fisher, B., et al. (2018). Improved retrievals of carbon dioxide from orbiting carbon observatory-2 with the version 8 ACOS algorithm. *Atmospheric Measurement Techniques*, *11*(12), 6539–6576. https://doi.org/10.5194/amt-11-6539-2018

Olson, M. E., Soriano, D., Rosell, J. A., Anfodillo, T., Donoghue, M. J., Edwards, E. J., et al. (2018). Plant height and hydraulic vulnerability to drought and cold. *Proceedings of the National Academy of Sciences of the United States of America*, *115*(29), 7551–7556. https://doi.org/10.1073/pnas.1721728115

Palmer, P. I., Feng, L., & Baker, D. (2019). Supplementary information for net carbon emissions from African land biosphere dominate pan-tropical atmospheric CO_2 signal.

Palmer, P. I., Feng, L., Baker, D., Chevallier, F., Bösch, H., & Somkuti, P. (2019). Dominate pan-tropical atmospheric CO_2 signal. *Nature Communications*, 1–9. https://doi.org/10.1038/s41467-019-11097-w

Pan, S., Pan, N., Tian, H., Friedlingstein, P., Sitch, S., Shi, H., et al. (2020). Evaluation of global terrestrial evapotranspiration using state-of-the-art approaches in remote sensing, machine learning and land surface modeling. *Hydrology and Earth System Sciences*, *24*(3), 1485–1509. https://doi.org/10.5194/hess-24-1485-2020

Parazoo, N. C., Bowman, K., Frankenberg, C., Lee, J.-E., Fisher, J. B., Worden, J., et al. (2013). Interpreting seasonal changes in the carbon balance of southern Amazonia using measurements of X_{CO2} and chlorophyll fluorescence from GOSAT. *Geophysical Research Letters*, *40*(11), 2829–2833. https://doi.org/10.1002/grl.50452

Pastorello, G., Trotta, C., Canfora, E., Chu, H., Christianson, D., Cheah, Y. W., et al. (2020). The FLUXNET2015 dataset and the ONEFlux processing pipeline for eddy covariance data. *Scientific Data*, *7*(1), 225. https://doi.org/10.1038/s41597-020-0534-3

Phillips, O. L., Aragão, L. E. O. C., Lewis, S. L., Fisher, J. B., Lloyd, J., López-González, G., et al. (2009). Drought sensitivity of the Amazon rainforest. *Science*, *323*(5919), 1344LP–1347. https://doi.org/10.1126/science.1164033

Phillips, O. L., Roel, J. W. B., & RAINFOR collaboration. (2017). Carbon uptake by mature Amazon forests has mitigated Amazon nations' carbon emissions. *Carbon Balance and Management*, *12*(1), 1. https://doi.org/10.1186/s13021-016-0069-2

Pokhrel, Y., Felfelani, F., Satoh, Y., Boulange, J., Burek, P., Gädeke, A., et al. (2021). Global terrestrial water storage and drought severity under climate change. *Nature Climate Change*, *11*(3), 226–233. https://doi.org/10.1038/s41558-020-00972-w

Pokhrel, Y. N., Fan, Y., & Miguez-Macho, G. (2014). Potential hydrologic changes in the Amazon by the end of the 21st century and the groundwater buffer. *Environmental Research Letters*, *9*(8), 84004. https://doi.org/10.1088/1748-9326/9/8/084004

Ruehr, N. K., Grote, R., Mayr, S., & Arneth, A. (2019). Beyond the extreme: Recovery of carbon and water relations in Woody plants following heat and drought stress (pp. 1285–1299). https://doi.org/10.1093/treephys/tpz032

Ryu, Y., Berry, J. A., & Baldocchi, D. D. (2019). What is global photosynthesis? History, uncertainties and opportunities. *Remote Sensing of Environment*, *223*, 95–114. https://doi.org/10.1016/j.rse.2019.01.016

Saatchi, S., Asefi-Najafabady, S., Malhi, Y., Aragão, L. E. O. C., Anderson, L. O., Myneni, R. B., & Nemani, R. (2013). Persistent effects of a severe drought on Amazonian forest canopy. *Proceedings of the National Academy of Sciences of the United States of America*, *110*(2), 565–570. https://doi.org/10.1073/pnas.1204651110

Saatchi, S. S., Harris, N. L., Brown, S., Lefsky, M., Mitchard, E. T. A., Salas, W., et al. (2011). Benchmark map of forest carbon stocks in tropical regions across three continents. *Proceedings of the National Academy of Sciences of the United States of America*, *108*(24), 9899–9904. https://doi.org/10.1073/pnas.1019576108

Salazar-Martínez, D., Holwerda, F., Holmes, T. R. H., Yépez, E. A., Hain, C. R., Alvarado-Barrientos, S., et al. (2022). Evaluation of remote sensing-based evapotranspiration products at low-latitude eddy covariance sites. *Journal of Hydrology*, *610*, 127786. https://doi.org/10.1016/j.jhydrol.2022.127786

Saleska, S. R., Rocha, H. R. D. A., Huete, A. R., Nobre, A. D., Artaxo, P. E., & Shimabukuro, Y. E. (2013). LBA-ECO CD-32 flux tower network data compilation, Brazilian Amazon: 1999-2006 [Dataset]. *ORNL Distributed Active Archive Center*. https://doi.org/10.3334/ORNLDAAC/1174

Schneider, D. P., Deser, C., Fasullo, J., & Trenberth, K. E. (2013). Climate data guide spurs discovery and understanding [Dataset]. *Eos, Transactions American Geophysical Union*, *94*(13), 121–122. https://doi.org/10.1002/2013EO130001

Stuart-Haëntjens, E., De Boeck, H. J., Lemoine, N. P., Mänd, P., Kröel-Dulay, G., Schmidt, I. K., et al. (2018). Mean annual precipitation predicts primary production resistance and resilience to extreme drought. *Science of the Total Environment*, *636*, 360–366. https://doi.org/10.1016/j.scitotenv.2018.04.290

Sulman, B. N., Roman, D. T., Yi, K., Wang, L., Phillips, R. P., & Novick, K. A. (2016). High atmospheric demand for water can limit forest carbon uptake and transpiration as severely as dry soil. *Geophysical Research Letters*, *43*(18), 9686–9695. https://doi.org/10.1002/2016GL069416

Sun, Y., Frankenberg, C., Wood, J. D., Schimel, D. S., Jung, M., Guanter, L., et al. (2017). OCO-2 advances photosynthesis observation from space via solar-induced chlorophyll fluorescence. *Science*, *358*(6360), eaam5747. https://doi.org/10.1126/science.aam5747

Tang, X., Li, H., Desai, A. R., Nagy, Z., Luo, J., Kolb, T. E., et al. (2014). How is water-use efficiency of terrestrial ecosystems distributed and changing on Earth? *Scientific Reports*, *4*(1), 7483. https://doi.org/10.1038/srep07483

Ukkola, A. M., De Kauwe, M. G., Roderick, M. L., Abramowitz, G., & Pitman, A. J. (2020). Robust future changes in meteorological drought in CMIP6 projections despite uncertainty in precipitation. *Geophysical Research Letters*, *47*(11), e2020GL087820. https://doi.org/10.1029/2020GL087820

Wigneron, J.-P., Fan, L., Ciais, P., Bastos, A., Brandt, M., Chave, J., et al. (2020). Tropical forests did not recover from the strong 2015–2016 El Niño event. *Science Advances*, *6*(6), eaay4603. https://doi.org/10.1126/sciadv.aay4603

Wilcox, K. R., Koerner, S. E., Hoover, D. L., Borkenhagen, A. K., Burkepile, D. E., Collins, S. L., et al. (2020). Rapid recovery of ecosystem function following extreme drought in a South African Savanna Grassland. *Ecology*, *101*(4), e02983. https://doi.org/10.1002/ecy.2983

Xu, L., Saatchi, S. S., Yang, Y., Yu, Y., Pongratz, J., Bloom, A. A., et al. (2021). Changes in global terrestrial live biomass over the 21st century. *Science Advances*, *7*(27), eabe9829. https://doi.org/10.1126/sciadv.abe9829

Xue, Q., Weiss, A., Arkebauer, T. J., & Baenziger, P. S. (2004). Influence of soil water status and atmospheric vapor pressure deficit on leaf gas exchange in field-grown winter wheat. *Environmental and Experimental Botany*, *51*(2), 167–179. https://doi.org/10.1016/j.envexpbot.2003.09.003

Yang, Y., Guan, H., Batelaan, O., Mcvicar, T. R., Long, D., Piao, S., et al. (2016). Contrasting responses of water use efficiency to drought across global terrestrial ecosystems. https://doi.org/10.1038/srep23284

Yang, Y., Saatchi, S. S., Xu, L., Yu, Y., Choi, S., Phillips, N., et al. (2018). Post-drought decline of the Amazon carbon sink. *Nature Communications*, *9*(1), 3172. https://doi.org/10.1038/s41467-018-05668-6